Urban Climate 40 (2021) 101026

Contents lists available at ScienceDirect

Urban Climate

journal homepage: www.elsevier.com/locate/uclim

A new approach to study the long-term urban heat island evolution using time-dependent spectroscopy

Svetlana A. Varentsova [a], Mikhail I. Varentsov [b,c,d,*]

[a] Faculty of Computational Mathematics and Cybernetics, Lomonosov Moscow State University, 1-52 Leninskiye Gory, 119992 Moscow, Russia
[b] Research Computing Centre, Lomonosov Moscow State University, 1/4 Leninskiye Gory, 119234 Moscow, Russia
[c] Faculty of Geography, Lomonosov Moscow State University, 1 Leninskiye Gory, 119991 Moscow, Russia
[d] Moscow Center for Fundamental and Applied Mathematics, 1 Leninskie Gory, 119991 Moscow, Russia

A R T I C L E I N F O

Keywords:
Urban heat island
Urban climate
Climate change
Spectral analysis
Time-depended spectroscopy
Fourier spectrum

A B S T R A C T

This study presents a new approach to study long-term temperature and urban heat island intensity (UHII) evolution based on the method of time-depended spectroscopy on the example of Moscow megacity. In contrast to standard spectroscopy, this method allows analyzing the changes of the amplitude Fourier spectrum of the time series along the study period. Applying the novel method to the air temperature series for the period of 1977-2020, we demonstrate that ongoing changes of the mean temperature and UHII are accompanied by the changes of their spectra, including the spectral amplitudes corresponding to diurnal, annual and synoptic-scale oscillations. Such changes are complex, often non-linear, and seasonally asymmetric. Steady upward trends are found for summer season, for the spectral amplitudes of diurnal temperature and UHII oscillations, and synoptic-scale UHII oscillations. Spectral amplitudes of annual temperature and UHII oscillations experiences V-shaped dynamics with an increase since 1990th. For UHII such pattern reflects a switch between regimes with wintertime or summertime UHI maximum. Presented results provides an evidence that observed intensification of Moscow's UHI is forced not only by urban growth, but also by changing background meteorological conditions, which are becoming more favorable to UHI appearance in summer and less favorable in winter.

1. Introduction

The climate change remains among the most important topics of the atmospheric sciences issues for the recent decades. The problems of climate change monitoring, prediction and mitigation is especially important for the urban areas. Firstly, the cities are the hotspots of climate warming, which is accelerated there by the urban heat island (UHI) effect and its amplification, induced by urban growth and development. UHI is defined as the air temperature excess in a city compared to the surrounding background areas, which appears due to land cover modifications, emissions of heat and pollutants, and other anthropogenic factors. UHI effect is studied in numerous papers and books, e.g. see the reviews in (Oke et al., 2017; Rizwan et al., 2008). The tendency of UHI amplification when the city growths and develops is documented for many regions, e.g. for Japanese cities (Fujibe, 2011), Beijing, China (Ren et al., 2007), New-York, USA (Gaffin et al., 2008), Manchester, UK (Levermore et al., 2018), Nur-Sultan, Kazakhstan (Berlessova and Konstantinov, 2020), Istambul, Turkey (Ünal et al., 2020). Secondly, the cities are particularly vulnerable to climate change and high-impact weather

* Corresponding author at: Research Computing Centre, Lomonosov Moscow State University, 1/4 Leninskiye Gory, 119234 Moscow, Russia.
E-mail address: mikhail.varentsov@srcc.msu.ru (M.I. Varentsov).

https://doi.org/10.1016/j.uclim.2021.101026
Received 8 July 2021; Received in revised form 13 October 2021; Accepted 31 October 2021

events as places where population and infrastructure are concentrated. Moreover, such vulnerability can be further increased by the local climate features. For example, in hot weather, UHI additionally amplifies the human heat stress, which can lead to increased mortality (Buechley et al., 1972; Gabriel and Endlicher, 2011; Tan et al., 2010).

Monitoring and understanding of the urban climate changes, including those ones induced by the city growth and development, are important for urban planning and climate change mitigation. However, it is not easy to quantify the contribution of the local-scale processes such as urbanization and larger-scale climate changes to the observed signal, because the local climate features such as UHI are highly sensitive to meteorological conditions and may be affected by the changes of their climatology.

Most of the regional climate change studies, including those ones focused on the UHI evolution, typically consider mean annual temperatures, or temperatures averaged over specific seasons, months, or times of the day. However, such means could not give the full information about the fluctuations of the analyzed phenomena, which may be critically important for the physical interpretation of observed changes. Powerful tools to analyze the phenomenon's fluctuations and their amplitudes are provided by the spectroscopy methods (Bell, 1972).

The power spectrum of a phenomenon describes the way in which the probable amplitudes of fluctuations depend on timescale (Bloomfield and Nychka, 1992). The concept of a spectrum is highly important in the atmospheric science. It underlies the division of atmospheric processes by scales, as well as the basis of the contemporary theory of atmospheric turbulence, that originate from the works of Kolmogorov, Monin and Obukhov (the review of this works and explanation of the theory may be found e.g. in (Foken, 2008)). The spectral approach is also a key tool for understanding the variability of the climate system in a wide range of temporal and spatial scales, see e.g. (Mitchell, 1976). Different methods to calculate the power spectra are provided for climatological tasks (Schickedanz and Bowen, 1977). The most common way of applying the spectral methods is to compute the spectra or a so-called periodogram (squared spectra) of global, regionally averaged or local climatic time series, e.g. for the mean global temperature (Bloomfield and Nychka, 1992) for a time series observed on a single site (Fredriksen and Rypdal, 2016; Paskota et al., 2013). Such periodograms are further used to understand the patterns of the temporal variability. Periodograms, computed for different sites or regions, can provide a useful information for the regional climate analysis. For example, Leite and Peixoto (1995) used spectral approach for climatic zoning of the Duero basing, and Weber and Talkner (2001) compared temperature spectra for mountainous and maritime observational sites. Nevertheless, applications of the spectral approach remain rare in the regional climate studies. They are especially rare in the field of urban climatology. One of the examples of applying spectral methods in urban climatology is a study of Kim and Baik (2004), which compared the spectral properties of UHI intensity in a number of Korean cities.

Spectral methods can supplement climate studies not only by stationary periodograms, but also provide valuable information about the temporal evolution of the phenomena's variability patterns. Such information can be assessed by applying the time-dependent spectroscopy methods, which are used in different scientific areas. For example, they are used in astrophysics (Mirabal et al., 2002), in biomedical applications (Vaks et al., 2012; Wilson et al., 1992). In the non-destructive inspection they can reveal, for example, defects in metal-oxide-semiconductor field effect transistors (Grasser et al., 2010). One of the time-dependent spectroscopy methods is a spectral dynamics analysis (SDA) method, which has demonstrated high efficiency in the field of THz time-domain spectroscopy and was successfully used for the detection and identification of various substances by using broadband THz pulse under laboratory and real conditions (Trofimov and Varentsova, 2015, 2016, 2019; Trofimov et al., 2018). However, our literature review has not revealed any relevant publications where the time-dependent spectroscopy methods were applied in climate studies.

This paper is aimed to demonstrate opportunities of application of the spectral approach, based on the SDA method, in the field of urban climate research on example of the Moscow megacity in Russia. Due to the size and compact city shape, the city experiences the intense UHI with urban-rural temperature differences reaching up to 14 °C (Lokoshchenko, 2014). Moscow megacity has already served as a test-bed for numerous urban climate studies based on observations, modelling and remote sensing, e.g. (Kuznetsova et al., 2017; Lokoshchenko and Enukova, 2020; Varentsov et al., 2018; Ivanovich et al., 2019). Recent studies have already documented the trend of UHI intensification in Moscow (Kislov, 2017; Kislov et al., 2017; Lokoshchenko, 2017). According to the results of recent studies, from 1977 to 2016, the annual urban-rural temperature difference increased from 1.6° to 2 °C, with especially pronounced increase in summer (Kislov, 2017; Kislov et al., 2017). However, previous studies do not provide a clear understanding of the physical drivers of such trends. In this paper, the time-dependent spectroscopy method is used to study in more details the long-term evolution of the Moscow UHI and possible reasons for its increase over the past decades.

2. Data and methods

2.1. Study area

Moscow is the biggest Russian and European monocentric urban agglomeration with population about approximately 17 million people (Cox, 2017), including population of Moscow city as federal subject of Russia and surrounding satellite cities in Moscow Oblast federal subject. The actual area of the city (excluding the suburbs and undeveloped areas) is about 1000 km^2. The city experienced intensive and almost linear population growth in second half of XX century as well in XXI century. During four recent decades, the population of Moscow administrative unit has increased by 65% from 7.6 million in 1976 to 12.5 million in 2020. Comparable rates of population growth could be assumed for the rest part of agglomeration. Population growth was accompanied by urban sprawl and increase of building height and density in all parts of the city except its historical center.

Moscow has a temperate humid, moderately continental climate (Dfb in Köppen climate classification) with mean annual temperature of 5.8 °C., mean June and January temperatures of 19.2 °C and − 6.5 °C, respectively (values are given for VDNKh weather station, that is typically used to characterize Moscow climate, for the 1981–2010 period). Due to the cold winters, Moscow is known as one of the world's coldest megacities. As typical for Eastern Europe, weather in Moscow experiences pronounced synoptic-scale variations both in summer and winter due to alteration of temperate, arctic, and tropical weather masses.

2.2. Meteorological data

Our study is based on the long-term and regular observational data at the weather stations in Moscow region, operated by the Russian national hydrometeorological service (Roshydroment). In total, we use data from 10 weather stations (Fig. 1a). The Balchug station (WMO ID 27605) was selected to represent the urban climate. It is located in a densely built area just in the historical city center of Moscow, in less than 1 km from Kremlin (Fig. 1b, c). Long-term meteorological observations are also available for a few other stations within Moscow megacity (Kislov, 2017; Lokoshchenko, 2014; Ivanovich et al., 2019; Varentsov et al., 2020a, 2020b), however they are located within heterogeneous surroundings in urban parks, and only Balchug is located in the quasi-homogeneous built environment. It experiences higher temperatures than other urban weather stations and represents a hotspot of the Moscow UHI (Ivanovich et al., 2019; Varentsov et al., 2020a, 2020b). In terms of the popular Local Climate Zones (LCZs) classification (Stewart and Oke, 2012), Balchug weather station represents LCZ 2 "compact midrise". To characterize the background conditions, we used the data for 9 stations surrounding the city, namely Klin (WMO ID 27417), Dmitrov (WMO ID 27419), Pavlovsky Posad (WMO ID 27523), Novo-Jerusalim (WMO ID 27511), Naro-Fominsk (WMO ID 27611), Serpukhov (WMO ID 27618), Kolomna (WMO ID 27625), Maloyaroslavets (WMO ID 27606), Aleksandrov (WMO ID 27428). These stations are further referred as rural neither they may be affected by local anthropogenic effects due to their location close to smaller towns or within rural/suburban settlements. Such selection of background weather stations is in line with several previous urban climate studies for Moscow (Kislov, 2017; Varentsov et al., 2018; Ivanovich et al., 2019; Varentsov et al., 2020a, 2020b).

The observational data set, used in the study, was compiled from the archives of All-Russia Research Institute of Hydrometeorological Information, World Data Centre, Hydrometeorological Research Center of Russian Federation and Central Administration of Hydrological and Environmental Monitoring. Based on data availability, the period from 1977 to 2020 was selected for our study. Temperature observation data is available with a 3-h discreteness, for timing 0, 3, 9, 12, 15, 18, 21 h in UTC time. Unfortunately, temperature time series include some gaps (periods of missing data). Although the missing data ratio for selected stations does not exceed 2% (with maximum length of one gap of 195 days found for Novo-Jerusalim in 1999–2000), we used a comprehensive regression-based gap-filling algorithm based on ideas from (Tardivo and Berti, 2012) to obtain continuous and homogeneous time series. Each individual gap for a specific station was filled based on a multiple linear regression using temperature observations at

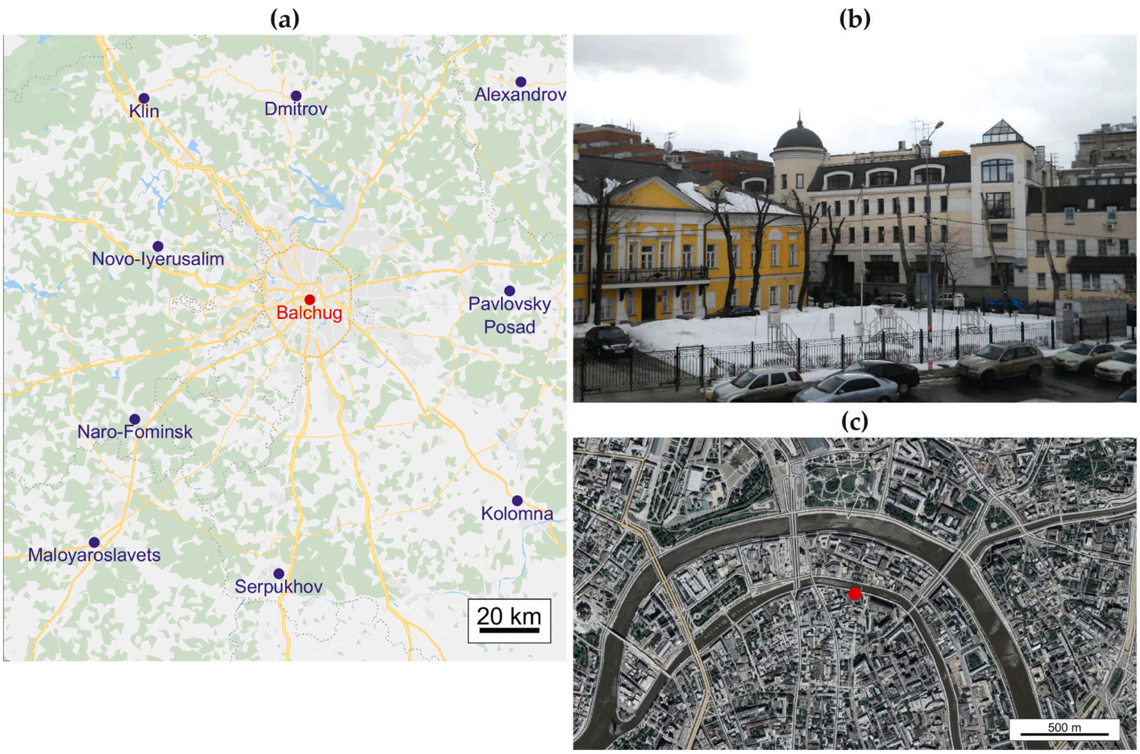

Fig. 1. Location of rural weather stations (blue points) and urban weather station Balchug, used in our study (a). Photo (b) shows Balchug weather station in winter, and piece of satellite image from Google maps (c) represents the local-scale surroundings of this station. (For interpretation of the references to colour in this figure legend, the reader is referred to the web version of this article.)

neighboring stations as predictors (a set from 3 to 5 neighboring stations were used that provide the best regression result). Gap-filling involved observations from all existing stations in the Moscow region in addition to 10 further used in this study. Regression coefficients were derived based on the data before and after each individual gap, separately for each hour of the day.

Further analysis is performed for the time series of $T_{urb}(t)$, $T_{rur}(t)$ and urban heat island intensity (UHII) $\Delta T(t) = T_{urb}(t) - T_{rur}(t)$, where $T_{urb}(t)$ is the temperature measured in the center of Moscow at the Balchug weather station, $T_{rur}(t)$ for each moment of time is defined as the average temperature over 9 selected rural weather stations.

2.3. Basics of the spectral dynamics analysis (SDA) method

The novel part of our study lies in the use of spectral dynamics analysis (SDA) method to analyze the patterns of temporal variations of temperature and UHI intensity, and their evolution over time under changing climate conditions. Here we give a brief introduction to the basics of the spectral analysis, including the SDA method.

Let $T(t)$ be a temperature time series obtained in the time interval $L_T = [t_b, t_e]$, where t_b and t_e are its beginning and the end. Then the Fourier transform of temperature $T(t)$ in the time interval length L_T is performed in the following way:

$$P(\nu) = \frac{1}{L_T}\int_{t_b}^{t_e} T(t)\cdot e^{-i2\pi\nu t}dt \tag{1}$$

where the complex spectral function $P(\nu)$ may be written as:

$$P(\nu) = \frac{1}{L_T}\left(P_1(\nu) + iP_2(\nu)\right) \tag{2}$$

The values:

$$|P(\nu)| = \frac{1}{L_T}\sqrt{P_1^2(\nu) + P_2^2(\nu)} \tag{3}$$

represent the amplitude Fourier spectrum of the temperature oscillations $T(t)$ in the observation time interval length L_T. In Section 3 we analyze the amplitude spectrum of temperature oscillations $T_{urb}(t)$, $T_{rur}(t)$ and $\Delta T(t) = T_{urb}(t) - T_{rur}(t)$ in the long time interval 1977–2020.

Note that in a number of works, for example in (Bloomfield and Nychka, 1992; Fredriksen and Rypdal, 2016; Leite and Peixoto, 1995; Paskota et al., 2013), the so-called periodograms are analyzed. The periodogram (or power spectrum) is defined as follows:

$$S(\nu) = \frac{1}{L_T}\left(P_1^2(\nu) + P_2^2(\nu)\right) = |P(\nu)|^2\cdot L_T \tag{4}$$

In comparison with the amplitude spectrum (3), the periodogram (4) provides a higher contrast of spectral data. However, the positions of the extremes of spectral functions $|P(\nu)|$ (3) and $S(\nu)$ (4) coincide. Amplitude spectra as well as periodograms are used to identify the dominant periods (or frequencies) of cyclic oscillations in the time series. This can be a helpful tool for identifying the dominant cyclical behavior.

In contrast to stationary spectroscopy, the time-depended spectroscopy method, namely, SDA-method, allows to analyze the temporal evolution of the spectral features along the given time series. In our study SDA method is applied for series $T_{urb}(t)$, $T_{rur}(t)$ and $\Delta T(t)$. Below we give the main notations and formulas at the construction of the evolution of the spectral amplitude of the temperature series $T(t)$ at the chosen frequency ν inthe time interval $L_T = [t_b, t_e]$ (Trofimov and Varentsova, 2015, 2016, 2019; Trofimov et al., 2018).

For this purpose, the selected time interval with length $L_{TW} < L_T$ (also called the time window) is shifted along the corresponding temperature series $T(t)$ by the value Δ_W (hereinafter referred to as the window shift) until the right end of the window coincides with the end of the observation time interval $L_T = [t_b, t_e]$. In order to prevent the spreading of the spectrum, in each time window with length L_{TW} the temperature series $T(t)$ is multiplied by window function $g(t)$ (Gabor function), which quickly tends to zero at the left and right ends of the window. This means that the values of the function $T(t)g(t)$ at the right and left ends of the time window become equal to zero (and to each other): $T(t_j)g(t_j)=T(t_{j+}L_{TW})g(t_{j+}L_{TW}) = 0$. Thus, the Fourier-Gabor transform is performed at the selected frequency ν:.

$$P(\nu t_j) = \frac{1}{L_{TW}}\int_{t_j}^{t_j+L_{TW}} T(t)\cdot g(t)e^{-i2\pi\nu\left(t-t_j\right)}dt,\ g(t) = e^{-\left(\frac{t-t_{c,j}}{0.5L_{TW}}\right)^n} \tag{5}$$

Here the point $t_j = t_b+(j-1)\Delta_W$ is a j-th window beginning, $t_{c,\,j} = t_j+0.5L_{TW}$ is a middle point of j-th window, $j = 1, \ldots, N$ is a serial number of window. $L_{TW} = N_{TW}h_t$ is a length of a time window, h_t is a time step or time discreteness. In our study, $h_t = 3$ h $= 0.125$ d. Parameter n was taken to be equal to 20 for window function $g(t)$ to fall off sharply at both ends of the window.

The spectral amplitude value $|P_\nu(t_j)|$ in the j-th time window is associated with the middle of this window:

$$|P_\nu(t_j)| = \left|P\left(\nu, t_j + 0.5L_{TW}\right)\right| = \left|P\left(\nu, t_{j+1} - 0.5L_{TW}\right)\right|, j = 1, \ldots, N \tag{6}$$

To start the computations, the first window is placed on time interval $[t_b, t_b + L_{TW}]$, and the last window has to coincide with the time interval $[t_e - L_{TW}, t_e]$.

A detailed method for constructing the evolution of the spectral amplitude is described in (Trofimov and Varentsova, 2015, 2016, 2019; Trofimov et al., 2018) as a part of the spectral dynamics analysis method (SDA-method).

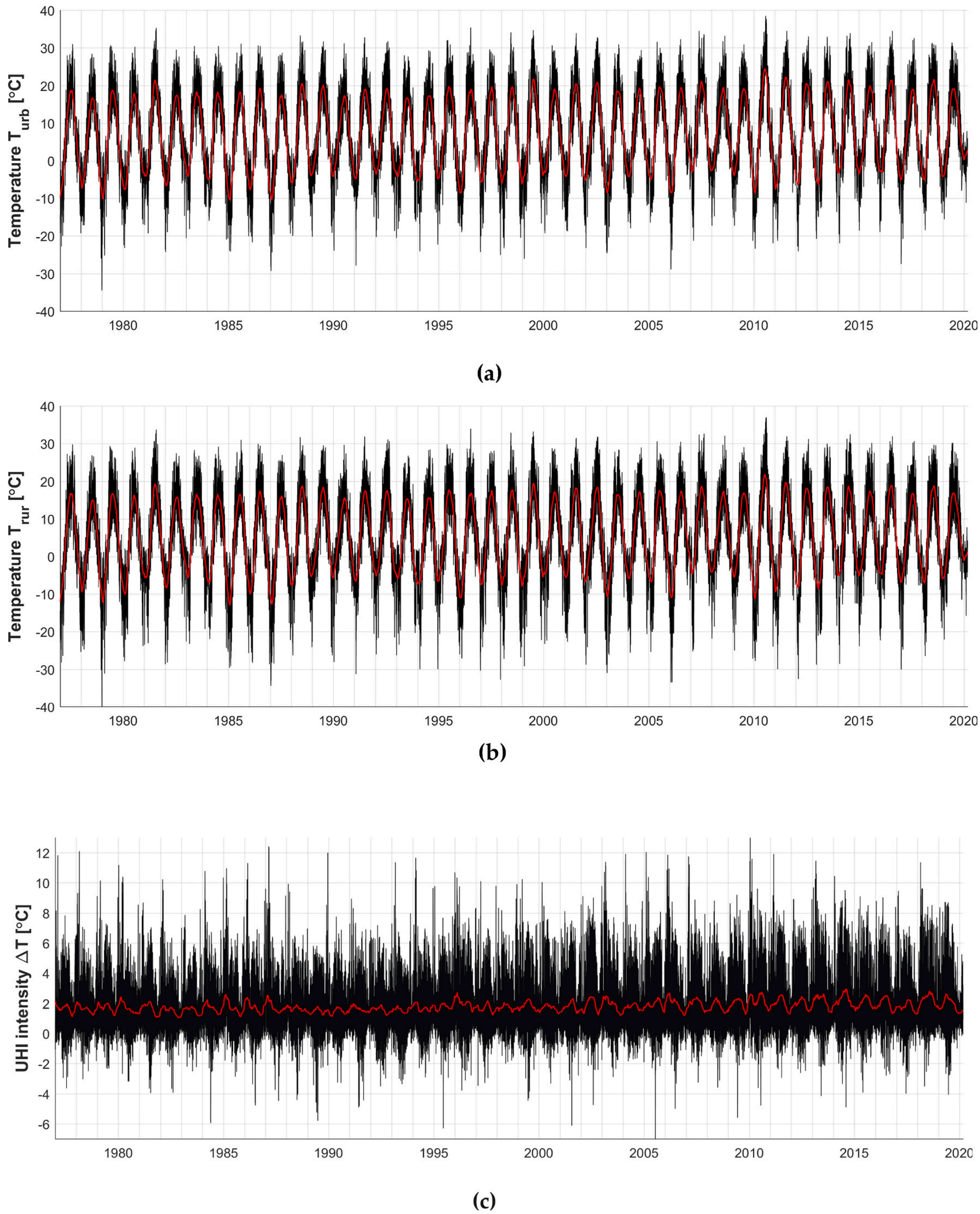

Fig. 2. Temperature oscillations in Moscow city $T_{urb}(t)$ (a) and for rural background $T_{rur}(t)$ (b), urban heat island intensity (UHII) $\Delta T(t) = T_{urb}(t) - T_{rur}(t)$ (c) in the time interval 1977–2020. Red lines indicate 3-month (90 days) running mean. (For interpretation of the references to colour in this figure legend, the reader is referred to the web version of this article.)

2.4. Data sampling and processing

We analyze the amplitude spectra of the temperature oscillations $T_{urb}(t)$, $T_{rur}(t)$ and $\Delta T(t)$ on the entire period of 1977–2020. For 2020, temperature data is available from January to April inclusive. The total duration of the observation time interval is 43 years and 4 months (15,826 days). One day (24 h) is taken as a unit of time measurement.

The raw time series, used in spectral analysis, are presented in Fig. 2. Both figures (a) and (b) clearly show 43 periods corresponding to the annual temperature course. As expected, the temperature oscillations $T_{urb}(t)$ (a) have the same shape as $T_{rur}(t)$ (b), but they lie higher on the temperature axis by an average of 1–3C°. Fig. 2 (c) shows $\Delta T(t)$ time series with a mean value of 1.79C° and extremes reaching more than 10 °C. The absolute UHII maximum is 13.2 °C, it was observed on January 19, 2010 at 06:00 UTC, when the temperature in the center of Moscow was −13.7 °C and mean background temperature was −26.9 °C. In contrast to temperature, UHII annual course is not so steady, and its evolution is further analyzed in our study.

Prior to applying spectral analysis, we consider the variations of the mean annual, summer (June–August) and winter (December–February) urban/rural temperatures and UHI intensity.

3. Result

3.1. Long term trends of the temperature and UHI intensity

Before analyzing the spectral characteristics of the temperature and UHII in Moscow region, it is essential to present the key patterns of the long-term evolution of these parameters. Here we briefly present such results, modified and updated after several recent studies (Kislov, 2017; Kislov et al., 2017; Varentsov et al., 2020a, 2020b).

Time-series of the annual and seasonal-averaged temperature for 1977–2020 demonstrate warming trends, which are consistent with numerous previous studies (Fig. 3a-c). The growth of the mean annual temperatures during this period is almost linear, with a linear trend coefficient k equal to 0.52 and 0.64 °C/10 years for T_{rur} and T_{urb} respectively. Variations of summer and winter

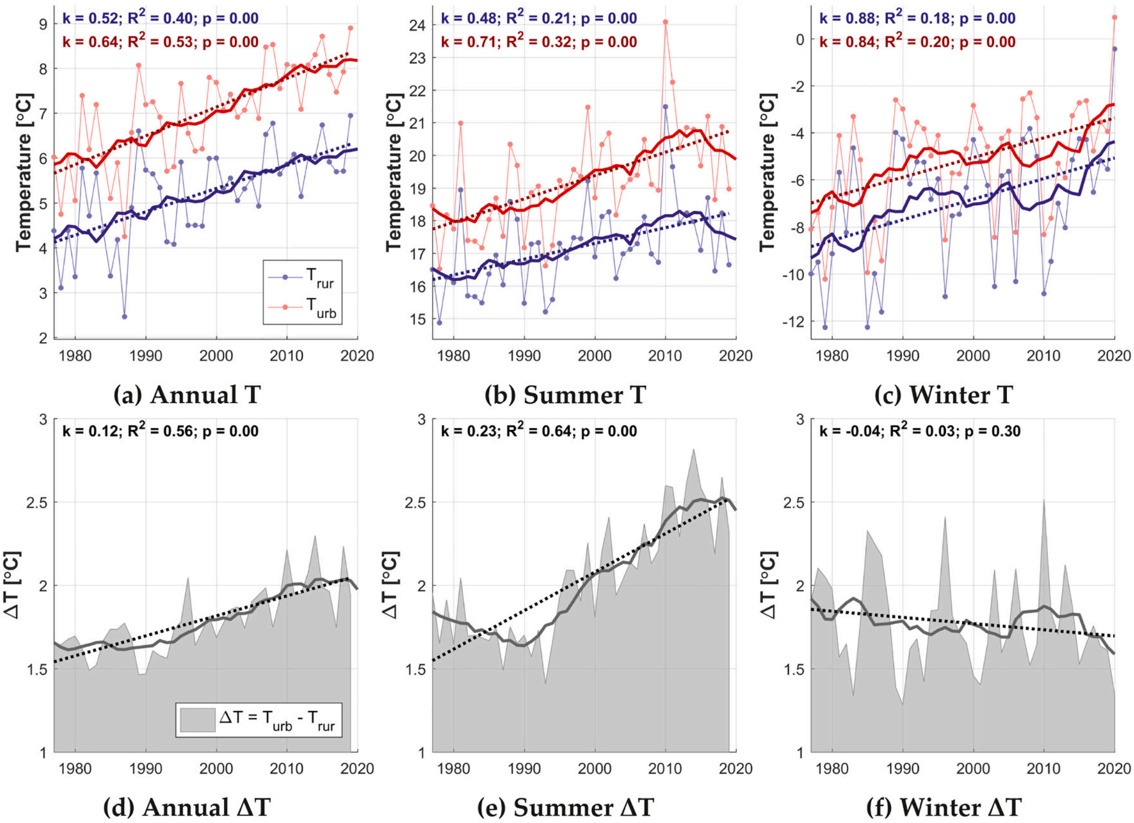

Fig. 3. Variations of the mean annual (a, d), summer (b, e) and winter (c, f) values of urban and rural temperatures (a-c) and urban heat island intensity ΔT (d-e) (in gray shading) over the period of 1977–2020. The bold lines indicate 10-year running means, dotted lines indicate linear trends. In the left corner of each plot, slope coefficient of the linear trend k, trend determination coefficient R^2 and confidence level p, at which the trend would be statistically significant by the Student's criterion, are presented.

temperatures demonstrate more complicated patterns. The most intense growth of summer temperatures was observed from 1990th to 2010th, however it was followed by a slowdown in growth and even a decrease in the 10-year average temperature after 2015th. In winter, on contrary, the most intense growth was observed before 1990th and after 2000th. The average rural warming speed is higher for winter (0.88 °C/decade) than for summer (0.48 °C/decade), however trend significance is comparable due to the higher inter-annual variability in winter.

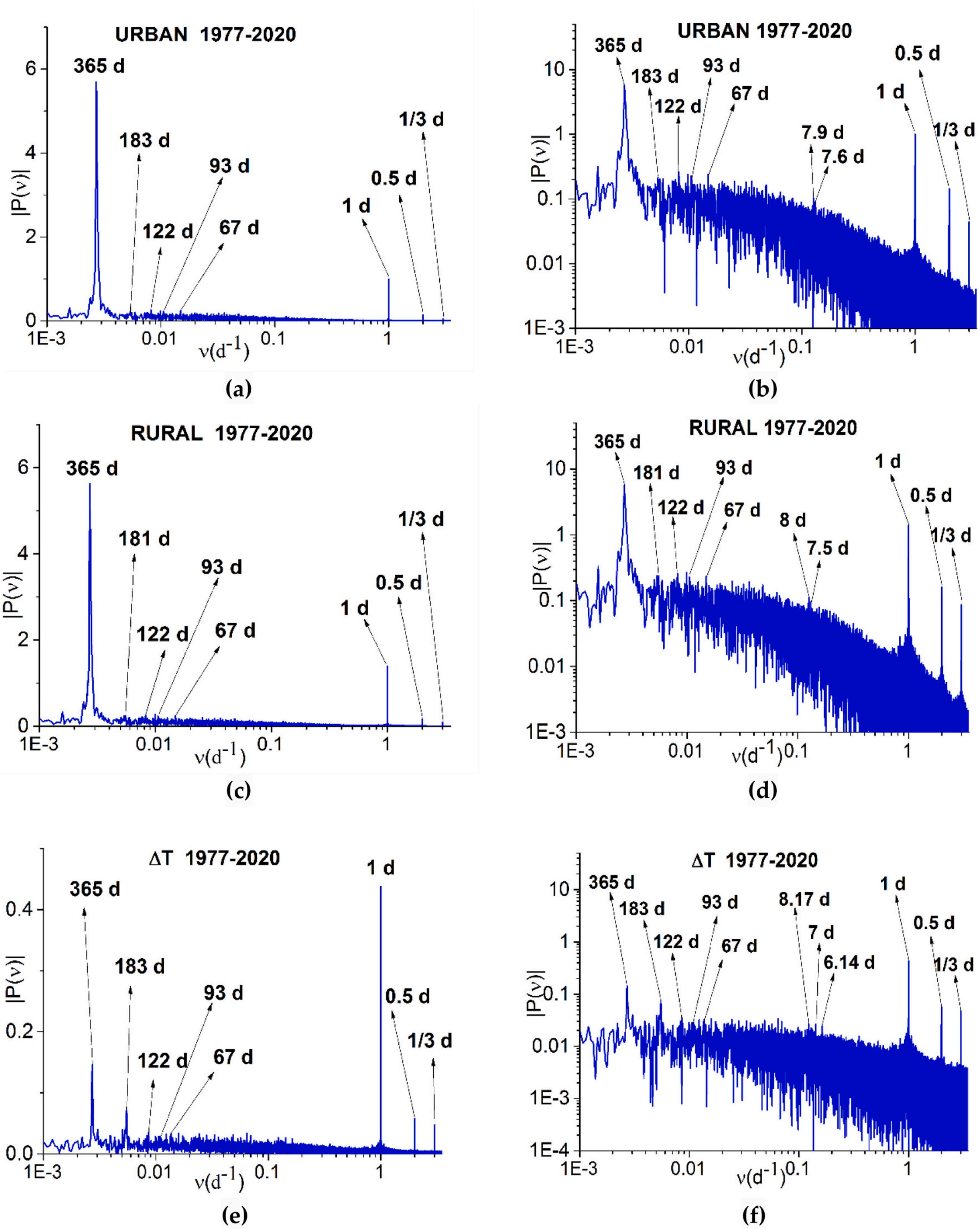

Fig. 4. Fourier spectrum of temperature oscillations $T_{urb}(t)$ (Moscow) (a), (b), $T_{rur}(t)$ (Moscow region) (c), (d) and UHII $\Delta T(t)$ (e), (f) in the time interval 1977–2020 in a logarithmic scale along the frequency axis (a), (c), (e) and along both axes (b), (d), (f).

The annual-mean UHII clearly (Fig. 3d) demonstrate an increasing trend with growth rate of 0.12 °C/decade, which resulted in 23% higher warming rate for the city center in comparison to rural background, representing the so-called urban-induced amplification of global warming (Kislov et al., 2017). The annual-mean UHII increased from 1.6 °C for first decade of analyzed period (1977–1986) to 2 °C for the last decade (2010–2019). Variations of the summer and winter UHII demonstrate inconsistent and more complicated dynamics (Fig. 3e, f). Summer UHII is growing twice faster than annual-mean UHII, but with a clearly expressed nonlinear dynamics. Summer UHII was steady, with even a slight tendency to decrease, in 1980th, then experienced a rapid growth from 1990 to 2010, and then stabilized around current maximum. Winter UHII demonstrates higher inter-annual variations with an insignificant ($p = 0.3$) decreasing trend. It worth to note that inter-annual variations of winter temperature and UHII are in anti-phase, i.e. lower winter temperature corresponds to higher winter UHII, which is further discussed in Section 3.3.

It is important to note that UHII dynamics is quite smooth and is not affected by sharp one-sided changes. Hence, observed dynamics is unlikely to be associated with changes in land cover and building properties in the local vicinity of urban weather station. Indeed, Balchug weather station is located in historical city center, where only limited developments took place during the study period. Hence, observed dynamics may be forced by growth and development of the whole Moscow megacity and by long-term changes of the background meteorological forcing.

3.2. Analysis of the amplitude spectra in the time interval 1977–2020

To study the spectral characteristics of $T_{urb}(t)$, $T_{rur}(t)$ and $\Delta T(t)$ oscillations, their Fourier amplitude spectra were obtained on the entire study period of 1977–2020. In Fig. 4 (a), (c), (d) the corresponding spectral amplitude $|P(\nu)|$ is shown in the logarithmic scale along the frequency axis and in the logarithmic scale along both axes for convenience in Fig. 4 (b), (d), (f).

When interpreting amplitude spectra plots, the primary attention should be paid to the dominant peaks that stand out from the background noise. These peaks indicate frequencies of the most pronounced cyclic oscillations in the analyzed time series. In all spectra of temperature oscillations $T_{urb}(t)$ (Fig. 4a,b), $T_{rur}(t)$ (Fig. 4c,d) and $\Delta T(t)$ (Fig. 4e,f), three peaks are clearly seen at the frequencies $\nu = 1/365$, 1.0, 2.0 d^{-1}, which correspond to oscillations with the period L_t=365 days (1 year), 1 day (24 h) and 0.5 days (12h). Logarithmic scale in Fig. 4 (b, d, f) allows detecting a maximum at the frequency ν=3.0 d^{-1}, which corresponds to oscillations with a period L_t=1/3 days = 8 h.

Not surprisingly, for urban and rural temperatures, the annual course (oscillations with a period of L_t=365 days) possesses the maximal spectral amplitude at the frequency ν=1/365 d^{-1}. The maximal contribution to the UHII $\Delta T(t)$ is made by oscillations with a period of one day ($\nu = 1.0$ d^{-1}), which is consistent with UHII spectra obtained for Korean cities (Kim and Baik, 2004) and with a typical UHII diurnal turn with its daytime minimum and nocturnal maximum (Oke et al., 2017). Oscillations at the frequencies ν=2.0 and 3.0 d^{-1} (i.e., L_t=0.5 days or 12 h, and 1/3 days or 8 h) reflects the deviations of the real diurnal temperature and UHII courses from the sine wave. Similarly, a small peak for a period about 181–183 days can be explained as a deviation of the annual course from the sine wave. The classic concepts of the temperature spectrum allow us to expect the presence of another spectral peak for the period of oscillations about 3–7 days corresponding to the synoptic-scale alteration of atmospheric processes (Griffith et al., 1956; Mitchell, 1976). Surprisingly, there are not any clearly expressed peaks of this period in our spectra. Minor peaks may be noticed in the panels (b), (d), (f) for the period about 7–8 days, yet they are very weak against the background noise. The absence of a pronounced peaks associated with synoptic-scale oscillations may be explained with a large spread in the duration of stable weather periods in Moscow region.

In the panels (b), (d), (f) one can also see a weak maximum for a period about 7 days, which is likely related to the dominant period of synoptic-scale alteration of atmospheric processes (Mitchell, 1976), and is further discussed below in Section 3.3.

Fig. 5 compares the spectral maxima max | $P_{urb}(\nu)$| and max | $P_{rur}(\nu)$| of the urban and rural temperature oscillations at the

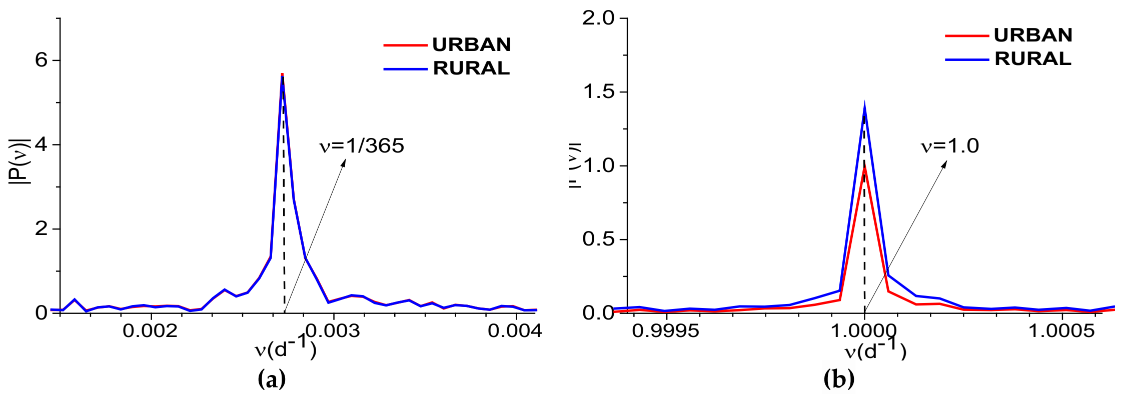

Fig. 5. Spectral maxima for temperature oscillations $T_{urb}(t)$ (Moscow) and $T_{rur}(t)$ (Moscow region) at the frequencies ν=1/365 d^{-1} (a) and ν=1.0 d^{-1} (b), corresponding to the annual and diurnal course, in the time interval 1977–2020.

frequencies ν=1/365 d^{-1} (a) and ν=1.0 d^{-1} (b), corresponding to the annual and diurnal course. The spectral maxima of the annual temperature course (a) are very close to each other: max | P_{urb}(1/365)| for the city is greater than max | P_{rur}(1/365)| by only 1.24%. For the diurnal temperature course, the background spectral maximum max | P_{rur}(1.0)| (b) is greater than urban spectral maximum max | P_{urb}(1.0)| by 39.5%. The later represents the interaction between well-known temperature and UHI diurnal cycles, i.e., the intense nocturnal UHI reduces diurnal temperature range in the city.

3.3. Analysis of the spectral amplitudes evolution in the time interval 1977–2020

The spectral characteristics considered above are averaged over a long-term time interval of 1977–2020, and therefore do not reflect changes that occurred within this period. To investigate such changes, we analyze the temporal evolution of the spectral amplitudes of $T_{urb}(t)$, $T_{rur}(t)$ and $\Delta T(t)$ oscillations at the frequencies corresponding to the annual (ν=1/365 d^{-1}) and diurnal (ν=1.0 d^{-1}) courses using SDA method with a running window of duration L_{TW}=10 years (3650 days) and the window shift Δ_W= 1 year (365 days).

For j-th window ($j = 1, \ldots, N$), the received spectral amplitude $|P_\nu(t_j)|$ is assigned to the time, corresponding to the window's center. For the first time interval L_{t1}=[1977, 1986] ($j = 1$), the obtained value of the spectral amplitude is defined as $|P_\nu(t_1)|=|P_\nu(1986 - 0.5L_{TW})| = |P_\nu(1981)|$. Since in 2020 temperature data are present only for the first four months, which is significantly less than the window shift Δ_W=1 year, we applied SDA method only for the data set cropped until 2019 incisively . In total, for the interval L_t=[1977, 2019] we get N=34 shifts of the window and corresponding values of $|P_\nu(t)|$, with a last time period L_{t34}=[2010, 2019], where $t_{34} = 2019 - 0.5L_{TW} = 2014$.

Since the UHI in a temperate city such as Moscow is controlled by different physical mechanisms in cold and warm seasons (Oke, 1982; Varentsov et al., 2020), it is essential to consider separately evolution of the temperature and UHI oscillations for contrasting summer and winter seasons. For this, SDA method was applied for "glued" time series of $T_{urb}{}^S(t)$, $T_{rur}{}^S(t)$ and $\Delta T^S(t)$ consisting from the data for three summer months (June, July, August) in the time interval 1977–2019; as well as series $T_{urb}{}^W(t)$, $T_{rur}{}^W(t)$ and $\Delta T^W(t)$ consisting of data for three winter months (December, January, February) in the interval 1977–2020. January and February 1977 were not included in the winter temperature series constructed in this way, since data for December 1976 are not available. Therefore, constructed "glued" series included data for 43 individual summer/winter seasons. SDA analysis was carried out again with a 10-year sliding time window (with L_{TW}= 900 days for winter and L_{TW}= 920 days for summer) shifted by one year (with Δ_W=90 days for winter and Δ_W=92 days for summer) along the corresponding summer/winter temperature series 1977–2019/2020.

Fig. 6 shows the evolution of the spectral amplitude $|P_\nu(t)|$ for temperature and UHII oscillations at the frequency ν=1/365 d^{-1}, corresponding to the annual course. Spectral amplitudes for temperature experience a non-linear V-shaped dynamics with a decrease in 1977–1997 (time points t_j=1981, …,1992 in panels (a), (b)), followed by an increase starting from the decade L_{t13}=[1989, 1998] (time point t_{13}=1993). Similar V-shaped pattern is observed for UHII (Fig. 6b). Comparing the spectral amplitudes values of UHII annual oscillations between the first and last decades (for L_{t1}=[1977, 1986], t_1=1981, and L_{t34}=[2010, 2019], t_{34}=2014), we get a relative increase by 40%.

The urban-rural difference in the spectral amplitudes of annual temperature oscillations is inconstant: annual temperature course is weaker in the city until 1990th, but then the city steadily overshadows the rural background with an increasing margin. Such a pattern clearly indicates a switch between contrasting regimes of UHI annual course with wintertime or summertime maxima, which is in line with results discussed in Section 3.1 (Fig. 3). In 1970th and 1980th the UHI was stronger in winter than in summer, resulting in lower annual spectral amplitude for $T_{urb}(t)$ than for $T_{rur}(t)$. The superiority of the summer UHII over the winter UHII has been increasing since the 1990th, also increasing the spectral amplitude of annual temperature oscillations the city. The period of switch between regimes with summer and winter UHII maxima corresponds to minimum of UHII spectral amplitude, which is observed at the decade

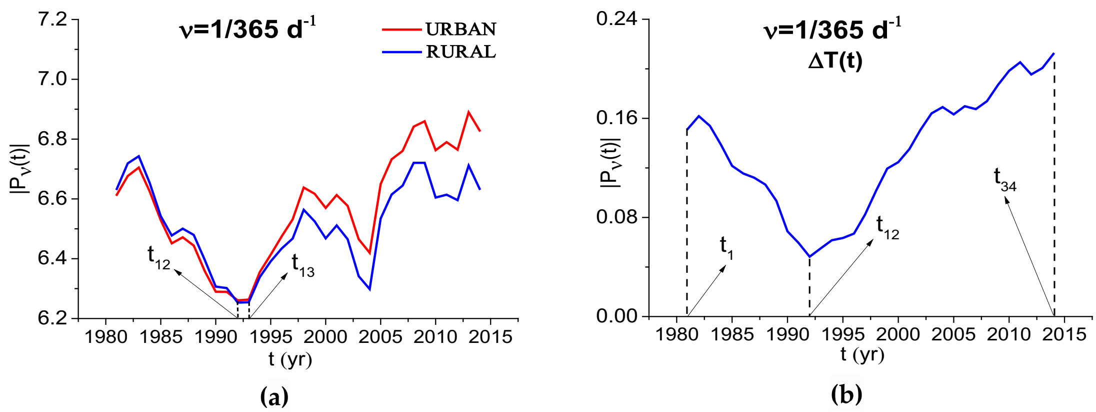

Fig. 6. Evolution of spectral amplitude $|P_\nu(t)|$ for the temperature oscillations $T_{urb}(t)$ and $T_{rur}(t)$ (a), for UHII $\Delta T(t)$ (b) at the frequency ν=1/365 d^{-1} corresponding to annual oscillations in the time interval L_T=[1977, 2019].

1988–1997 (t_{12}=1992 at Fig. 6b).

Evolution of the spectral amplitudes for diurnal temperature and UHII oscillations with ν=1.0 d^{-1} is shown in Fig. 7 for the whole year and separately for summer and winter seasons. On average for the whole year, the spectral amplitudes for $T_{rur}(t)$ stably exceed such amplitudes for $T_{urb}(t)$ on the entire time interval L_T= [1977, 2019] with an increasing margin (Figure 7a). Both spectral amplitudes experience an increasing trend, but amplitude for $T_{rur}(t)$ has increased by 10.1% between the first and last decades, and amplitude for $T_{urb}(t)$ has increased only by 2.5%. The amplitude of diurnal oscillation for UHII shows a stable increasing trend on entire study period (Fig. 7b). Comparison between the spectral amplitudes for the first and last decades gives a relative increase by 40%. Considering the increasing UHI trend, such result indicates the asymmetry of the warming rates for daytime and nighttime.

Spectral amplitudes of the diurnal temperature and UHII oscillations have different dynamics for summer and winter seasons.

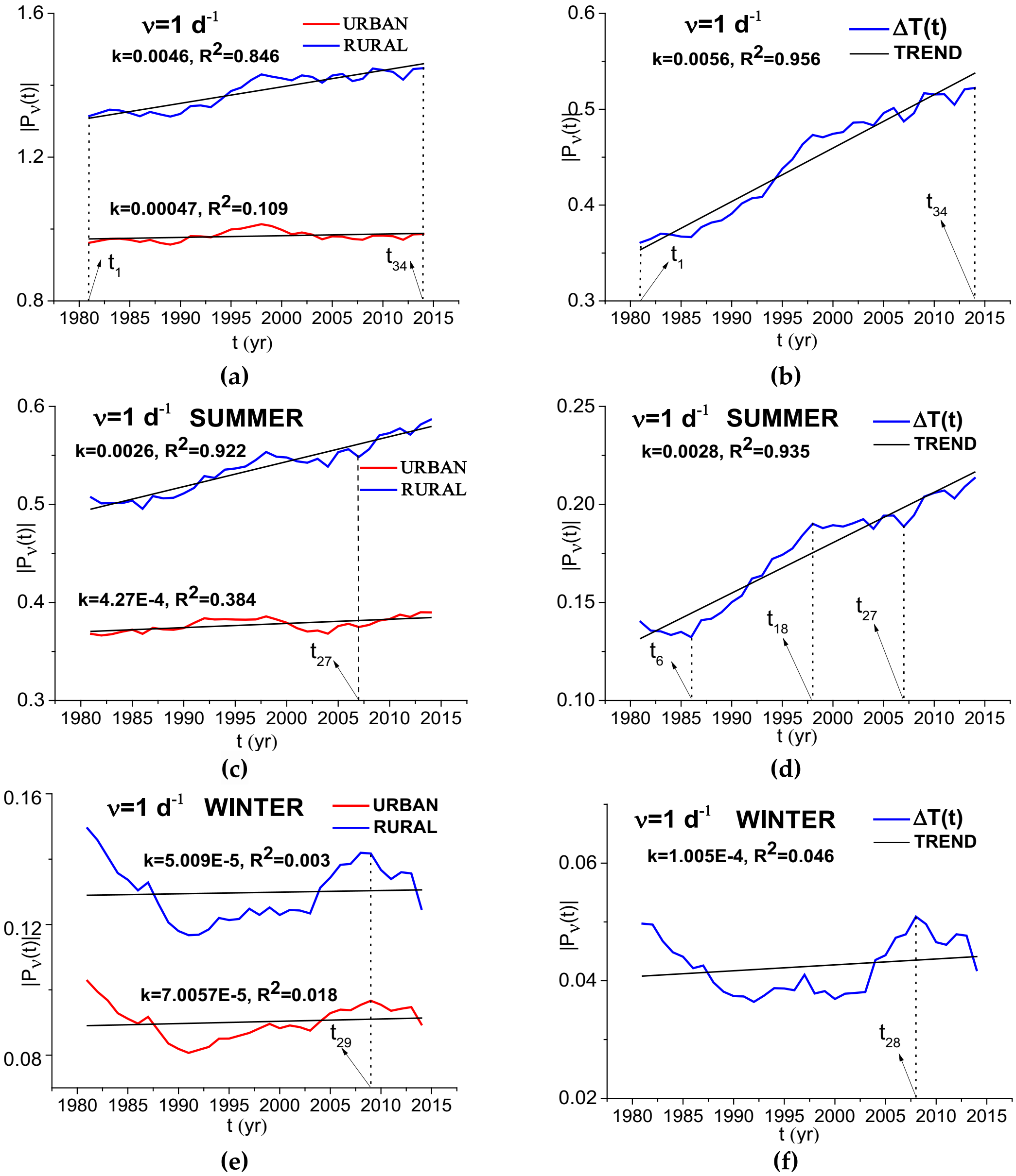

Fig. 7. Evolution of the spectral amplitude $|P_\nu(t)|$ for the oscillations of $T_{urb}(t)$, $T_{rur}(t)$ (a) and $\Delta T(t)$ (b) at the frequency ν=1 d^{-1} corresponding to diurnal oscillations, for summer oscillations of $T_{urb}{}^S(t)$, $T_{rur}{}^S(t)$ (c) and $\Delta T^S(t)$ (d), for winter oscillations of $T_{urb}{}^W(t)$, $T_{rur}{}^W(t)$ (e) and $\Delta T^W(t)$ (f) at the frequency ν=1 d^{-1} . The corresponding parameters are: L_{TW}=3650 (a, b), 920 (c, d) and 900 (e, f) days, Δ_W= 365 (a, b), 92 (c, d) and 90 (e, f) days, in the time interval L_T= [1977, 2019] (a-d), [1977, 2020] (e,f). For each plot, slope coefficient of the linear trend k and trend determination coefficient R^2 are presented.

Dynamics of summer spectral amplitudes repeats their average annual variations (Fig. 7c), but is much more pronounced, with a relative increase between first and last decades by 15.6 and 5.9% for $T_{rur}(t)$ and $T_{urb}(t)$, respectively. Hence, observed trends on the average annual scale are largely contributed by faster changes in summer. Increase of summer spectral amplitudes was paused in 2000th and continued since the decade 2003–2012 (time point t_{27}= 2007 in Fig. 7c) and up to the present. The spectral amplitude of summer UHII diurnal oscillation again follows the same patterns as for rural temperature (Fig. 7d), with increase periods observed from the decade 1982–1991 (time point t_6= 1986) up to the decade 1994–2003 (time point t_{18}= 1998) and after decade 2003–2012 (time point t_{27}= 2007), and with a relative increase between first and last decades of 52%.

For winter season, the spectral amplitudes of both urban and rural temperatures experience complicated dynamics with decrease in 1980th and 1990th, increase in 2000th and decrease since the decade 2005–2014 (time point t_{29}= 2009) to the present (Fig. 7e). The spectral amplitude of winter UHII diurnal oscillation follows the same pattern (Fig. 7f).

In addition to diurnal and annual cycles, the atmospheric processes in moderate and high latitudes experience significant variations on a so-called synoptic scale, i.e., with a period from first days to first weeks, associated with alteration of large-scale weather systems. UHI phenomena strongly depends on the background weather. It is well-expressed under calm and clear weather and may almost disappear under cloudy and windy weather conditions (Oke et al., 2017). Influence of the weather conditions on UHI intensity is well documented for many cities including Moscow (Varentsov et al., 2020a, 2020b; Yushkov et al., 2019).

Since the synoptic-scale processes do not have a regular period, they are not expressed as a single peak in temperature or UHII spectra in Fig. 4, with only a faintly discernible maximum traced for the period around 7 days. Zooming to a narrower frequency range $0.033 \leq \nu \leq 0.5$ d^{-1}, corresponding to oscillations with a period from 2 to 30 days (Fig. 8), allows considering this peak more closely on example of two periods, 1977–1986 and 2010–2019. To suppress the noise, here we smoothed the initial spectrum using the 5-points adjacent averaging. Both for rural temperature and UHII spectra, peaks with a period around 7 days are found against overall growth of spectral power with an increase of period length. Nevertheless, peaks for 7-day period remain dominant until the period L_t= 14 days for temperature (a, b), 30 days (c), 26 days (d) for UHII. For temperature, this peak is expressed much weaker than in classic study by Mitchel (1976), where synoptic maximum remains dominant until the period of 6 months.

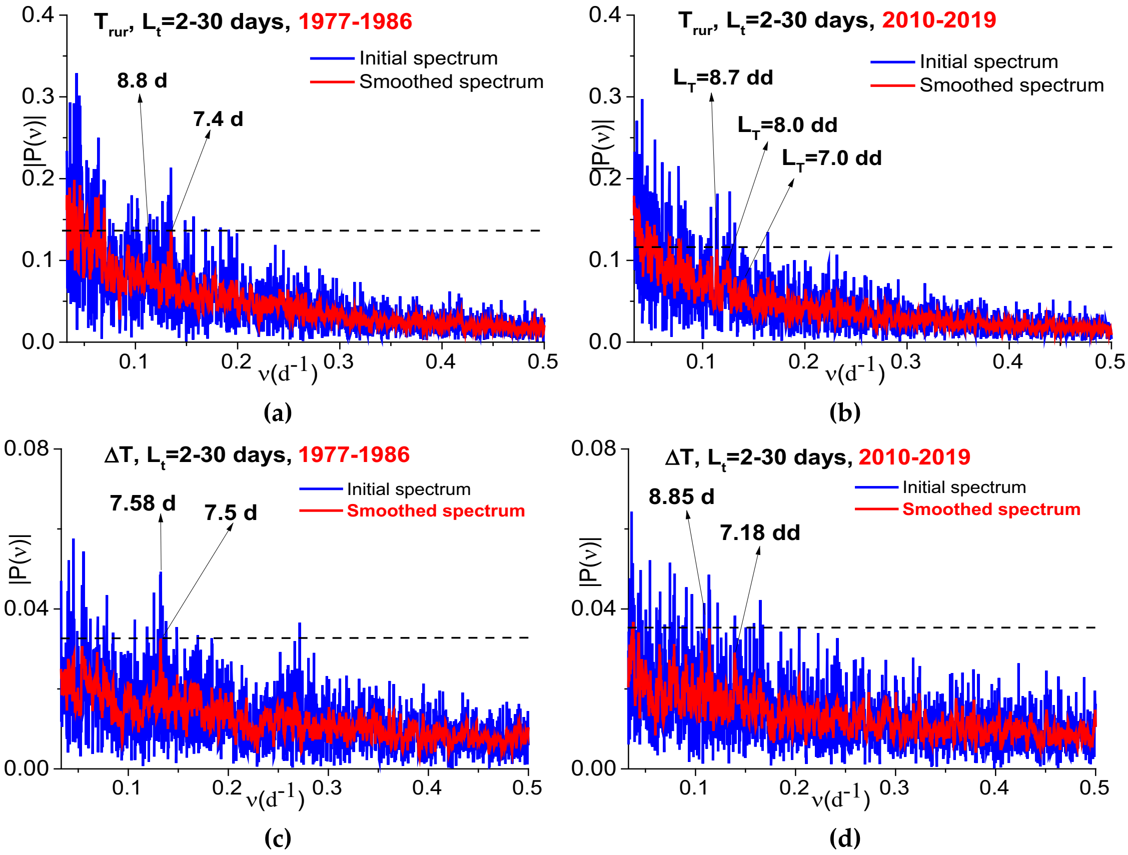

Fig. 8. Fourier spectrum of rural temperature $T_{rur}(t)$ (a, b) and UHII $\Delta T(t)$ (c, d) on the short time intervals duration 10 years 1977–1986 (a), (c) and 2010–2019 (b), (d) in the frequency range $0.033 \leq \nu \leq 0.5$ d^{-1} (c), (d) in a linear scale. Initial spectrum is shown in blue, the smoothed spectrum (5-points adjacent averaging) – in red. Horizontal dotted line indicates the spectral maximum found around 7 ± 2 day period. (For interpretation of the references to colour in this figure legend, the reader is referred to the web version of this article.)

For UHI intensity, the spectral maximum with 7-days period may be associated not only with alteration of synoptic processes, but also with weekly cycle of human activity. Previously the coherent, but statistically insignificant dependence between UHI intensity and day of the week was documented for Moscow by Lokoshchenko (2014). Comparing spectra for two periods shown in Figs. 8, 1977–1986 and 2010–2019, one may note that 7-day oscillation is stronger expressed for the first period. This may indicate a transition from industrial to post-industrial society but should be additionally analyzed in further studies.

To quantify the contribution of the synoptic-scale processes to the temperature and UHI oscillations and to track its temporal evolution within study period, we analyze the integral power in the frequency range $0.07 \leq \nu \leq 0.5$ d^{-1} corresponding to oscillations with the period from 2 to14 days. Using the same technique, which was applied for the computation of the evolution of spectral amplitude $|P_\nu(t_j)|$ at the chosen frequency ν (Eqs. (5), (6)), we can obtain the evolution of the integral power of temperature oscillations $W_\nu(t_j)$ corresponding to the selected frequency range. Taking into account that when computing the spectral amplitude $|P_\nu(t_j)|$ in each window length $L_{TW} = N_{TW}h_t$ it was already divided by factor N_{TW} (the discrete case of Eq.(5)), we obtain:

$$W_\nu(t_j) = 2\sum_{0.07 \leq \nu \leq 0.5} S_\nu(t_j) = 2N_{TW}\sum_{0.07 \leq \nu \leq 0.5} |P_\nu(t_j)|^2, \; j = 1, \dots, N \tag{11}$$

The factor 2 in Eq. (11) is due to the fact that for a real function $T(t)$ the discrete Fourier transform is even symmetric, so, the values $|P_\nu(t_j)|$ are completely specified by $N_{TW}/2$ time points.

In Fig. 9 the evolution of the "synoptic-scale" temperature oscillations power $W_\nu(t_j)$ is depicted for winter $T_{urb}{}^W(t)$, $T_{rur}{}^W(t)$ (a) and summer temperature series $T_{urb}{}^S(t)$, $T_{rur}{}^S(t)$ (b), winter UHII $\Delta T^W(t)$ (c) and summer UHII $\Delta T^S(t)$ (d) computed in the frequency range $0.07 \leq \nu \leq 0.5$ d^{-1} . The parameters of the computation are the same as described above for Fig. 7. In Fig. 9a one can see the decrease of the winter power both for urban and rural temperature starting from the decade 1996–2005 (time point t_{20}=2000). Such results indicate that winter weather is becoming less changeable in winter during last two decades, i.e. alterations of cold and warm weather is becoming weaker and/or rarer. The summer power (Fig. 9b) increases for urban temperatures, starting from the decade 1996–2005 (time point t_{17}=1997) with a maximum observed in the decade 2002–2011 (time point t_{26}=2006), while for rural temperature there are not any significant changes.

It is interesting to note that the power of winter oscillations is greater for rural than urban temperatures, and vice versa for summer

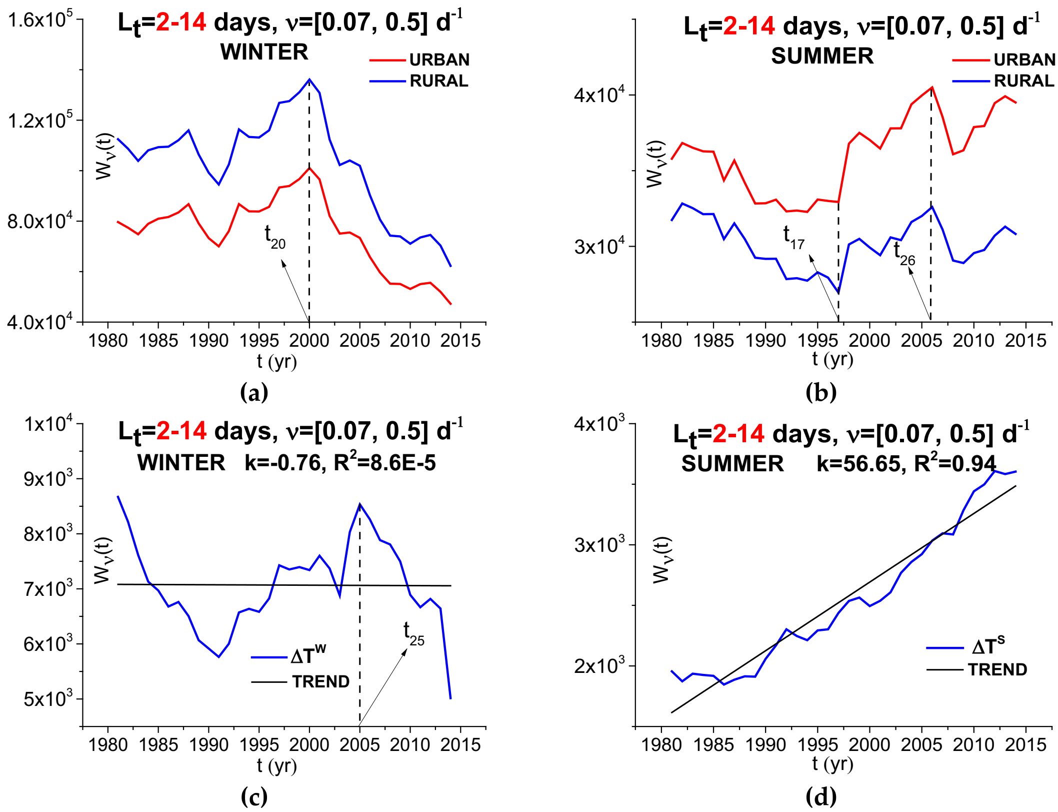

Fig. 9. Evolution of the integral power $W_\nu(t_j)$ for winter temperature oscillations $T_{urb}{}^W(t)$, $T_{rur}{}^W(t)$ (a), summer temperature oscillations $T_{urb}{}^S(t)$, $T_{rur}{}^S(t)$ (b), and UHII $\Delta T^W(t)$ (c), $\Delta T^S(t)$ (d) computed in the frequency range $0.07 \leq \nu \leq 0.5$ d^{-1} with parameters L_{TW}=900 (a), (c), 920 days (b), (d), Δ_W= 90 (a), (c), 92 days (b), (d) in the time interval L_T= [1977, 2020] (a), (c), [1977, 2019] (b), (d). For plots (c) and (d), slope coefficient of the linear trend k and trend determination coefficient R^2 are presented.

oscillations. This is not surprising, since the strongest winter UHIs in temperate and high-latitude cities typically follow frosty weather episodes or so-called cold waves (Fortuniak et al., 2006; Konstantinov et al., 2018; Yang and Bou-Zeid, 2018; Yushkov et al., 2019), resulting in a less pronounced temperature variations in the cities. This also explains the revealed anti-phase dynamics between mean winter temperate and UHII (Fig. 3). From a physical point of view, such dependence can be explained by an increase in anthropogenic heat flux from heated buildings, as well as by the trapping of released heat by the shallow stable boundary layer, the formation of which is typical for winter cold weather episodes in middle and high latitudes (Akhmetshina et al., 2014; Bourne et al., 2010; Yushkov et al., 2019). In summer, on contrast, UHIs tend to amplify during the warm weather, especially during the heat waves (De Ridder et al., 2016; Li and Bou-Zeid, 2013; Schatz and Kucharik, 2015), enhancing the variations of the daily-mean temperature with respect to rural areas.

The integral power of UHII synoptic-scale oscillations shows a steady increase for summer season with a relative increase of 84% within the study period (Fig. 9d), which corresponds to increase of spectral amplitudes by 35% according to Eq. (11). More complicated dynamics is observed for winter season, with a decrease in 1980th, increase in 1990th and decrease in recent years since decade 2000–2010 (Fig. 9b). Contrasting summer and winter patterns are generally close to those ones observed for diurnal oscillation amplitudes (Fig. 7), but here the amplification of UHII oscillations is largely contributed by increase of urban temperature oscillations.

The data analysis methods in our study are configured to analyze multi-year trends, and therefore do not allow detecting isolated extreme events such as heat/cold waves and intense UHI episodes. Nonetheless, revealed long-term trends allows suggesting the changes in climatology and behaviors of such events. Considering variations in the integral power of synoptic-scale oscillations of rural temperature and UHII (Fig. 9), as well as the fact of UHI intensification during heat waves in summer and cold waves in winter (discussed above), we could suggest that summer heat waves are becoming more frequent and/or more intense during the whole study period, and winter cold waves are becoming less frequent/less intense during the last two decades.

4. Discussion

The UHI is one of the clearest examples of inadvertent climate modification due to humans (Oke et al., 2017), which turns the cities to the hotspots of climate change. Higher rates of climate warming in comparison to rural areas are documented for several world's cities. Although UHI appearance is linked with background meteorological forcing (e.g. wind speed and cloudiness), which may be more or less favorable for UHI appearance (Hoffmann et al., 2012; Oke et al., 2017), faster urban warming is typically associated with urban sprawl and development (Berlessova and Konstantinov, 2020; Fujibe, 2011; Kalnay and Ming, 2003; Lokoshchenko, 2017). The possible impacts of the background forcing are often ignored in the UHI evolution studies, likely due to two reasons. Firstly, the representative long-term UHI observations are available only for a few world's cities. Secondly, the long-term UHI evolution studies typically consider only mean temperature values, averaged over seasons and years, so the changes of UHI temporal variations on smaller time scales remain masked.

The current study addresses the problem of the long-term UHI evolution on example of Moscow megacity for more than four recent decades (1977–2020). During this period, Moscow experienced population increase by 65%, intensive urban growth and development, pronounced warming of regional climate by 2 °C as well as increase of mean UHII for city center by 0.4 °C. The latter represents the so-called urban amplification of climate warming (Kislov et al., 2017).

In contrast to previous UHI evolution studies for Moscow and other world's cities, we focus not on the mean temperatures, but on the spectra of the urban/rural temperatures and their differences. To study evolution of these spectra, we apply the time-dependent spectroscopy method, which is popular tool for signal processing in different scientific areas but was not previously used in urban climatology or in regional climate changes in general. Application of the novel approach allows to reveal that the long-term changes of the mean UHII are accompanied by the changes of UHII amplitude Fourier spectrum. The UHII spectrum for Moscow has the dominant peaks corresponding to diurnal and annual oscillations, which is in line with physical expectations and with UHII spectra found for several Korean cities (Kim and Baik, 2004). However, we show for the first time that the amplitudes of such oscillations are inconstant and experience the long-term variations.

Spectral amplitude of annual UHII oscillations experiences the nonlinear V-shaped dynamics. It is associated with a transition between contrasting regimes with UHI maxima observed in winter (in 1970th and 1980th) and in summer (since 2000th), caused by seasonally asymmetric trends of the mean UHII. The switch between two regimes happened in 1990th and resulted in the decrease of spectral amplitude of annual UHII oscillations. Such changes cannot be explained by the urban growth and development, so they clearly indicate the impact of changes in background meteorological forcing. Results for annual UHI oscillations stand out from previous studies. Previously, ambiguous results on the UHI seasonal variations were reported for several mid- and high-latitude cities. Summer maxima of the mean UHI intensity was reported e.g. for Istambul in Turkey (Ünal et al., 2020), New-York (Gedzelman et al., 2003) and Madison in USA (Schatz and Kucharik, 2014), London in UK (Wilby, 2003), Lodz (Kłysik and Fortuniak, 1999) and Torun (Przybylak et al., 2017) in Poland, Turku (Suomi and Käyhkö, 2012) in Finland, while winter maximum was found for Beijing, China (Yang et al., 2013), Belgrade, Serbia (Unkašević et al., 2001), Seul, South Korea (Kim and Baik, 2005), and also in several cities in West Siberia (Miles and Esau, 2017) and Fennoskandia (Miles and Esau, 2020) according to remote sensing data. However, none of these studies analyzed the nonstationarity of the UHI annual course. Hence, listed ambiguous results may be associated not only with geographical differences, but also with differences in study periods and associated variability of the large-scale atmospheric forcing.

Presented results also show the nonstationarity of the UHII diurnal course, which spectral amplitude experiences steady upward trend and increased by 40% during study period. Together with upward trend for mean UHII, this allows speaking about the diurnal asymmetry of urban-amplified warming in Moscow, by analogy with the diurnal asymmetry of global warming revealed by Davy et al. (2017). Joint analysis of the diurnal oscillation spectral amplitudes for rural/urban temperatures and UHII suggests that the observed changes are again partially contributed by the variability of the background climatic conditions, which are becoming more favorable for UHI appearance in summer. The increase of UHII diurnal spectral amplitude is accompanied with fast increase of rural temperature spectral amplitudes, while urban temperature spectral amplitudes are increasing much slower. UHI intensity is well correlated with diurnal temperature range, which determines the nocturnal cooling potential for rural areas (Theeuwes et al., 2017). We cannot deny that the slower growth of the diurnal temperature amplitude in the city may be partially forced with its growth and development. Nonetheless, rural temperature range is evidently more sensitive to the changes in background meteorological forcing, so its faster increase under favorable weather conditions and resulted UHI intensification is expected even the urban properties are not changed.

In addition to diurnal and annual oscillations, we analyzed synoptic-scale oscillations of temperature and UHII, determined by alteration of weather conditions with a period of several days. In contrast to temperature spectra from classic work of Mitchell (1976) with a clear peak for the period of 3–5 days, we found only a weak and faintly discernible peak for a period of 7–8 days. For UHII, this peak may be partially related with a weekly cycle of human activity as suggested by Lokoshchenko (2014). In either case, such effect request more accurate investigation in further studies. Integral power of oscillations with periods from 2 to 14 days for temperature experiences nonlinear dynamics both in summer and winter, with a pronounced decrease for winter during the last two decades. Power of such oscillations for UHII in summer experiences steady upward trend, with a relative increase of corresponding spectral amplitudes by 35%. This mean that UHII increases for the days when it is already high and does not change for the days when UHI is not expressed. Considering the known fact of UHI amplification during summer heat waves (Li and Bou-Zeid, 2013) and winter cold waves (Yang and Bou-Zeid, 2018), observed dynamics may be partially associated with trends of repeatability and/or intensity of heat/cold wave, that should be analyzed in further studies.

Observed changes in temperature and UHII spectra are consistent with documented dynamics of other meteorological parameters in Moscow region. There is a downward trend in the summer cloudiness and decrease in overcast frequency in the European part of Russia according to observations at weather stations for 1990–2010 (Chernokulsky et al., 2011). Negative cloud cover trend in Moscow region is also revealed based on satellite data for 1984–2007 (Tang et al., 2012). The high-quality observations at the meteorological observatory of Lomonosov Moscow State University also show a downward trend in low cloud fraction and overcast frequency and an upward trend in sunshine frequency (Gorbarenko, 2019), as well as upward trend of direct solar radiation (Gorbarenko, 2016). At the same time, European part of Russia experiences downward wind speed trends, which is shown by several observational studies reviewed by (Wu et al., 2018). Such changes are expected to increase the frequency of calm and clear weather conditions, favorable for UHI appearance in summer. At the same time, there are not any significant changes in winter cloudiness in European part of Russia for 1990–2010 period (Chernokulsky et al., 2011). Moreover, the winters in Europe are generally becoming warmer, with increasing repeatability of extremely mind winters (Twardosz and Kossowska-Cezak, 2016). Decreasing repeatability of cold waves, which are favorable for winter UHI appearance, is also seen for Moscow since 2000th according to presented results. Changes in meteorological forcing can be related both with regional aspects of ongoing global climate change as well as by natural climate oscillations such as North Atlantic Oscillation (Iles and Hegerl, 2017), this question requires further investigation.

5. Conclusion

In this study, evolution of air temperature and urban heat island intensity (UHII) in Moscow megacity is analyzed based on long-term observations for the period of 1977–2020. In addition to analysis of annual and seasonal temperature and UHII means, we apply time-depended spectroscopy method to analyze the changes of the amplitude Fourier spectrum of the time series along the study period. The temperature and UHII spectra for Moscow are dominated by diurnal and annual oscillations, yet synoptic-scale oscillations are not expressed as a dominant spectral peak in contrast to classic studies. For the first time we show that temperature and UHII spectra are inconstant in time and experience the long-term variations. Observed changes of temperature and UHII regimes are complex, often non-linear, seasonally asymmetric, and include the following key patterns:

- Climate warming is clearly expressed in Moscow region. For rural areas, annual-mean warming rate is 0.52 °C per decade. Moscow city center experiences 23% faster warming (0.64 °C per decade) due to increasing UHII.
- UHII experiences seasonally asymmetric and non-linear dynamics. The mean growth rate of summer UHII (0.23 °C per decade) is twice higher that for annual-mean UHII (0.12 °C per decade), with the fastest changes observed from 1990 to 2010. The winter UHI experiences pronounced interannual variations without significant trend.
- Steady upward trends are found for the spectral amplitudes of diurnal oscillations of rural temperature and UHII, and synoptic-scale UHII oscillations in summer. The relative increase between first and last decades is 40% for diurnal UHII oscillations for the whole year and 52% for summer, 35% for synoptic-scale UHII oscillations in summer. Dynamics of the same spectral amplitudes is more complex and non-linear for winter, with a decreasing tendency for two last decades.
- Spectral amplitudes of annual temperature and UHII oscillations experiences V-shaped dynamics with an increase since 1990th. For UHII such pattern reflects a switch between regimes with wintertime or summertime UHI maximum.

Presented results provide an evidence that observed UHI evolution is a complex process, which is determined not only by urban growth and development, but also by long-term variations in the large-scale meteorological forcing and its favorability for UHI appearance. Hence, the nonstationary of meteorological forcing should not be ignored when discussing the urban-induced climate changes and designing urban climate projections.

Summing up, we could recommend the time-depended spectroscopy method as extremely useful and illustrative for analyzing long-term evolution of temperature and UHI intensity. In our opinion, this method is unfairly deprived of attention in urban climatology and regional climate research in general. In contrast to the analysis based on mean values, time-depended spectroscopy does not mask small-scale variations of analyzed phenomena and allows tracking dynamics of corresponding oscillations. Its application can make the research results for different regions more visual and facilitate their intercomparison.

Funding

The bulk of the study, including data processing and analysis was supported by Ministry of Education and Science of the Russian Federation, agreement No. 075–15–2021-574. Interpretation of spectral analysis results was supported by Ministry of Education and Science of the Russian Federation as part of the program of the Moscow Center for Fundamental and Applied Mathematics under the agreement №075–15–2019-1621. This research has been also supported by the Interdisciplinary Scientific and Educational School of Moscow University «Brain, Cognitive Systems, Artificial Intelligence».

Declaration of Competing Interest

The authors declare no conflict of interest.

References

Akhmetshina, A.S., Kizhner, L.I., Gorbatenko, V.P., Zuev, V.V., Shelekhov, A.P., Shelekhova, E.A., 2014. Some characteristics of inversions in Tomsk according to MTP-5 temperature profiler. In: *20th International Symposium on Atmospheric and Ocean Optics: Atmospheric Physics*, *9292*, 92924M. https://doi.org/10.1117/12.2075234.

Bell, R., 1972. *Introductory Fourier Transform Spectroscopy* (1st Editio). Academic Press, New York.

Berlessova, A.A., Konstantinov, P.I., 2020. Local climate zones in the city of Nur-sultan (Kazakhstan) and their connections with urban heat island and thermal comfort. IOP Conf. Ser. Earth Environ. Sci. 611 (1) https://doi.org/10.1088/1755-1315/611/1/012060.

Bloomfield, P., Nychka, D., 1992. Climate spectra and detecting climate change. Clim. Chang. 21 (3), 275–287. https://doi.org/10.1007/BF00139727.

Bourne, S.M., Bhatt, U.S., Zhang, J., Thoman, R., 2010. Surface-based temperature inversions in Alaska from a climate perspective. Atmos. Res. 95 (2–3), 353–366. https://doi.org/10.1016/j.atmosres.2009.09.013.

Buechley, R.W., Van Bruggen, J., Truppi, L.E., 1972. Heat island = death island? Environ. Res. 5 (1), 85–92. https://doi.org/10.1016/0013-9351(72)90022-9.

Chernokulsky, A.V., Bulygina, O.N., Mokhov, I.I., 2011. Recent variations of cloudiness over Russia from surface daytime observations. Environ. Res. Lett. 6 (3) https://doi.org/10.1088/1748-9326/6/3/035202.

Cox, W., 2017. Demographia World Urban Areas (World Agglomerations). *Wendel Cox Consultancy, Illinois* (13th Annua). Belleville, Illinois. Retrieved from. http://www.demographia.com/db-worldua.pdf.

Davy, R., Esau, I., Chernokulsky, A., Outten, S., Zilitinkevich, S., 2017. Diurnal asymmetry to the observed global warming. Int. J. Climatol. 37 (1), 79–93. https://doi.org/10.1002/joc.4688.

De Ridder, K., Maiheu, B., Lauwaet, D., Daglis, I., Keramitsoglou, I., Kourtidis, K., Manunta, P., Paganini, M., 2016. Urban Heat Island intensification during hot spells - the case of Paris during the summer of 2003. Urban Sci. 1 (1), 3. https://doi.org/10.3390/urbansci1010003.

Foken, T., 2008. Micrometeorology doi:10.1007978-3-540-74666-9.

Fortuniak, K., Kłysik, K., Wibig, J., 2006. Urban - rural contrasts of meteorological parameters in Łódź. Theor. Appl. Climatol. 84 (1–3), 91–101. https://doi.org/10.1007/s00704-005-0147-y.

Fredriksen, H.B., Rypdal, K., 2016. Spectral characteristics of instrumental and climate model surface temperatures. J. Clim. 29 (4), 1253–1268. https://doi.org/10.1175/JCLI-D-15-0457.1.

Fujibe, F., 2011. Urban warming in Japanese cities and its relation to climate change monitoring. Int. J. Climatol. 31 (2), 162–173. https://doi.org/10.1002/joc.2142.

Gabriel, K.M.A., Endlicher, W.R., 2011. Urban and rural mortality rates during heat waves in Berlin and Brandenburg, Germany. Environ. Pollut. 159 (8–9), 2044–2050. https://doi.org/10.1016/j.envpol.2011.01.016.

Gaffin, S.R., Rosenzweig, C., Khanbilvardi, R., Parshall, L., Mahani, S., Glickman, H., Goldberg, R., Blake, R., Slosberg, R.B., Hillel, D., 2008. Variations in New York city's urban heat island strength over time and space. Theor. Appl. Climatol. 94 (1–2), 1–11. https://doi.org/10.1007/s00704-007-0368-3.

Gedzelman, S.D., Austin, S., Cermak, R., Stefano, N., Partridge, S., 2003. Mesoscale aspects of the urban Heat Island around New York City. Sciences 42 (1), 29–42. https://doi.org/10.1007/s00704-002-0724-2.

Gorbarenko, E.V., 2016. Climate changes in atmospheric radiation parameters from the MSU meteorological observatory data. Russ. Meteorol. Hydrol. 41 (11−12), 789–797. https://doi.org/10.3103/S1068373916110078.

Gorbarenko, E.V., 2019. Sunshine variability in Moscow in 1955–2017. Russ. Meteorol. Hydrol. 44 (6), 384–393. https://doi.org/10.3103/S1068373919060037.

Grasser, T., Reisinger, H., Wagner, P.J., Kaczer, B., 2010. Time-dependent defect spectroscopy for characterization of border traps in metal-oxide-semiconductor transistors. Phys. Rev. B Condens. Matter Mater. Phys. 82 (24), 1–10. https://doi.org/10.1103/PhysRevB.82.245318.

Griffith, H.L., Panofsky, H.A., Van der Hoven, I., 1956. Power-spectrum analysis over large ranges of frequency. J. Meteorol. 13 (3), 279–282. https://doi.org/10.1175/1520-0469(1956)013<0279:PSAOLR>2.0.CO;2.

Hoffmann, P., Krueger, O., Schlünzen, K.H., 2012. A statistical model for the urban heat island and its application to a climate change scenario. Int. J. Climatol. 32 (8), 1238–1248. https://doi.org/10.1002/joc.2348.

Iles, C., Hegerl, G., 2017. Role of the North Atlantic oscillation in decadal temperature trends. Environ. Res. Lett. 12 (11) https://doi.org/10.1088/1748-9326/aa9152.

Ivanovich, Varentsov Mikhail, Grishchenko, M.Y., Wouters, H., 2019. Simultaneous assessment of the summer urban heat island in Moscow megacity based on *in situ* observations, thermal satellite images and mesoscale modeling. Geogr. Environ. Sustain. 12 (4), 74–95. https://doi.org/10.24057/2071-9388-2019-10.

Kalnay, E., Ming, C., 2003. Impact of urbanization and land-use change on climate. Nature 423 (May), 528–531. https://doi.org/10.1038/nature01649.1.

Kim, Y.H., Baik, J.J., 2004. Daily maximum urban heat island intensity in large cities of Korea. Theor. Appl. Climatol. 79 (3–4), 151–164. https://doi.org/10.1007/s00704-004-0070-7.

Kim, Y.-H., Baik, J.-J., 2005. Spatial and temporal structure of the urban Heat Island in Seoul. J. Appl. Meteorol. 44 (5), 591–605. https://doi.org/10.1175/JAM2226.1.

Kislov, A.V. (Ed.), 2017. Climate of Moscow in Conditions of Global Warming [in Russian]. Publishing house of Moscow University, Moscow.

Kislov, A.V., Varentsov, M.I., Gorlach, I.A., Alekseeva, L.I., 2017. "Heat island" of the Moscow agglomeration and the urban-induced amplification of global warming [in Russian]. *Moscow University Vestnik. Series 5.* Geography 4, 12–19.

Kłysik, K., Fortuniak, K., 1999. Temporal and spatial characteristics of the urban heat island of Łódź, Poland. Atmos. Environ. 33 (24–25), 3885–3895. https://doi.org/10.1016/S1352-2310(99)00131-4.

Konstantinov, P., Varentsov, M., Esau, I., 2018. A high density urban temperature network deployed in several cities of Eurasian Arctic. Environ. Res. Lett. 13 (7), 075007 https://doi.org/10.1088/1748-9326/aacb84.

Kuznetsova, I.N., Brusova, N.E., Nakhaev, M.I., 2017. Moscow urban Heat Island: detection, boundaries, and variability. Russ. Meteorol. Hydrol. 42 (5), 305–313. https://doi.org/10.3103/S1068373917050053.

Leite, S.M., Peixoto, J.P., 1995. Spectral analysis of climatological series in Duero Basin. Theor. Appl. Climatol. 50 (3–4), 157–167. https://doi.org/10.1007/BF00866114.

Levermore, G., Parkinson, J., Lee, K., Laycock, P., Lindley, S., 2018. The increasing trend of the urban heat island intensity. Urban Clim. 24, 360–368. https://doi.org/10.1016/j.uclim.2017.02.004.

Li, D., Bou-Zeid, E., 2013. Synergistic interactions between urban heat islands and heat waves: the impact in cities is larger than the sum of its parts. J. Appl. Meteorol. Climatol. 52 (9), 2051–2064. https://doi.org/10.1175/JAMC-D-13-02.1.

Lokoshchenko, M.A., 2014. Urban ‘heat island’ in Moscow. *Urban climate, 10*. Part 3, 550–562. https://doi.org/10.1016/j.uclim.2014.01.008.

Lokoshchenko, Mikhail A., 2017. Urban Heat Island and urban Dry Island in Moscow and their centennial changes. J. Appl. Meteorol. Climatol. 56 (10), 2729–2745. https://doi.org/10.1175/JAMC-D-16-0383.1.

Lokoshchenko, M., Enukova, E.A., 2020. Urban Heat Island in Moscow derived from satellite data. Russ. Meteorol. Hydrol. 45 (7), 488–497. https://doi.org/10.3103/S1068373920070043.

Miles, V., Esau, I., 2017. Seasonal and spatial characteristics of urban Heat Islands (UHIs) in northern west Siberian cities. Remote Sens. 9 (10), 989. https://doi.org/10.3390/rs9100989.

Miles, V., Esau, I., 2020. Surface urban heat islands in 57 cities across different climates in northern Fennoscandia. Urban Clim. 31 (August 2019), 100575. https://doi.org/10.1016/j.uclim.2019.100575.

Mirabal, N., Halpern, J.P., Kulkarni, S.R., Castro, S., Bloom, J.S., Djorgovski, S.G., Galama, T.J., Harrison, F.A., Frail, D.A., Price, P.A., Reichart, D.E., Ebeling, H., Bunker, A., Dawson, S., Dey, A., Spinrad, H., Stern, D., 2002. Time-dependent optical spectroscopy of GRB 010222: clues to the gamma-ray burst environment. Astrophys. J. 578 (2), 818–832. https://doi.org/10.1086/342619.

Mitchell, J.M., 1976. An overview of climatic variability and its causal mechanisms. Quat. Res. 6 (4), 481–493. https://doi.org/10.1016/0033-5894(76)90021-1.

Oke, T.R., 1982. The energetic basis of the urban heat island. Q. J. R. Meteorol. Soc. 108 (455), 1–24. https://doi.org/10.1002/qj.49710845502.

Oke, T.R., Mills, G., Christen, A., Voogt, J.A., 2017. Urban Climates. Cambridge University Press, Cambridge. https://doi.org/10.1017/9781139016476.

Paskota, M., Vujović, D., Todorović, N., 2013. Repetitiveness and underlying characteristics of climatologic parameters in winter. Theor. Appl. Climatol. 113 (1–2), 317–328. https://doi.org/10.1007/s00704-012-0788-6.

Przybylak, R., Uscka-Kowalkowska, J., Araźny, A., Kejna, M., Kunz, M., Maszewski, R., 2017. Spatial distribution of air temperature in Toruń (Central Poland) and its causes. Theor. Appl. Climatol. 127 (1–2), 441–463. https://doi.org/10.1007/s00704-015-1644-2.

Ren, G.Y., Chu, Z.Y., Chen, Z.H., Ren, Y.Y., 2007. Implications of temporal change in urban heat island intensity observed at Beijing and Wuhan stations. Geophys. Res. Lett. 34 (5), 1–5. https://doi.org/10.1029/2006GL027927.

Rizwan, A.M., Dennis, L.Y.C., Liu, C., 2008. A review on the generation, determination and mitigation of urban Heat Island. J. Environ. Sci. 20 (1), 120–128. https://doi.org/10.1016/S1001-0742(08)60019-4.

Schatz, J., Kucharik, C.J., 2014. Seasonality of the urban heat island effect in Madison, Wisconsin. J. Appl. Meteorol. Climatol. 53 (10), 2371–2386. https://doi.org/10.1175/JAMC-D-14-0107.1.

Schatz, J., Kucharik, C.J., 2015. Urban climate effects on extreme temperatures in Madison, Wisconsin, USA. Environ. Res. Lett. 10 (9), 094024 https://doi.org/10.1088/1748-9326/10/9/094024.

Schickedanz, P.T., Bowen, E.G., 1977. The computation of climatological power spectra. J. Appl. Meteorol. 16 (4), 359–367. https://doi.org/10.1175/1520-0450(1977)016<0359:TCOCPS>2.0.CO;2.

Stewart, I.D., Oke, T.R., 2012. Local climate zones for urban temperature studies. Bull. Am. Meteorol. Soc. 93 (12), 1879–1900. https://doi.org/10.1175/BAMS-D-11-00019.1.

Suomi, J., Käyhkö, J., 2012. The impact of environmental factors on urban temperature variability in the coastal city of Turku, SW Finland. Int. J. Climatol. 32 (3), 451–463. https://doi.org/10.1002/joc.2277.

Tan, J., Zheng, Y., Tang, X., Guo, C., Li, L., Song, G., Zhen, X., Yuan, D., Kalkstein, A.J., Li, F., Chen, H., 2010. The urban heat island and its impact on heat waves and human health in Shanghai. Int. J. Biometeorol. 54 (1), 75–84. https://doi.org/10.1007/s00484-009-0256-x.

Tang, Q., Leng, G., Groisman, P.Y., 2012. European hot summers associated with a reduction of cloudiness. J. Clim. 25 (10), 3637–3644. https://doi.org/10.1175/JCLI-D-12-00040.1.

Tardivo, G., Berti, A., 2012. A dynamic method for gap filling in daily temperature datasets. J. Appl. Meteorol. Climatol. 51 (6), 1079–1086. https://doi.org/10.1175/JAMC-D-11-0117.1.

Theeuwes, N.E., Steeneveld, G.J., Ronda, R.J., Holtslag, A.A.M., 2017. A diagnostic equation for the daily maximum urban heat island effect for cities in northwestern Europe. Int. J. Climatol. 37 (1), 443–454. https://doi.org/10.1002/joc.4717.

Trofimov, V.A., Varentsova, S.A., 2015. An effective method for substance detection using the broad spectrum THz signal with a Terahertz Nose. Sensors (Switzerland) 15 (6), 12103–12132. https://doi.org/10.3390/s150612103.

Trofimov, V.A., Varentsova, S.A., 2016. Detection and identification of drugs under real conditions by using noisy terahertz broadband pulse. Appl. Opt. 55 (33), 9605. https://doi.org/10.1364/ao.55.009605.

Trofimov, V.A., Varentsova, S.A., 2019. A possible way for the detection and identification of dangerous substances in ternary mixtures using thz pulsed spectroscopy. Sensors (Switzerland) 19 (10), 1–35. https://doi.org/10.3390/s19102365.

Trofimov, V.A., Varentsova, S.A., Yang, Y., 2018. Detection and identification of a substance with an inhomogeneous surface using the effective time-dependent thz spectroscopy method and emission frequency up-conversion. EPJ Web Conf. 195 https://doi.org/10.1051/epjconf/201819509005.

Twardosz, R., Kossowska-Cezak, U., 2016. Exceptionally cold and mild winters in Europe (1951–2010). Theor. Appl. Climatol. 125 (1–2), 399–411. https://doi.org/10.1007/s00704-015-1524-9.

Ünal, Y.S., Sonuç, C.Y., Incecik, S., Topcu, H.S., Diren-Üstün, D.H., Temizöz, H.P., 2020. Investigating urban heat island intensity in Istanbul. Theor. Appl. Climatol. 139 (1–2), 175–190. https://doi.org/10.1007/s00704-019-02953-2.

Unkašević, M., Jovanović, O., Popović, T., 2001. Urban-suburban/rural vapour pressure and relative humidity differences at fixed hours over the area of Belgrade city. Theor. Appl. Climatol. 68 (1–2), 67–73. https://doi.org/10.1007/s007040170054.

Vaks, V.L., Domracheva, E.G., Sobakinskaya, E.A., Chernyaeva, M.B., Maslennikova, A.V., 2012. Using the methods and facilities of nonsteady-state spectroscopy of the subterahertz and terahertz frequency ranges for noninvasive medical diagnosis. J. Opt. Technol. 79 (2), 66. https://doi.org/10.1364/JOT.79.000066.

Varentsov, M., Wouters, H., Platonov, V., Konstantinov, P., 2018. Megacity-induced Mesoclimatic effects in the lower atmosphere: a modeling study for multiple summers over Moscow, Russia. Atmosphere 9 (2), 50. https://doi.org/10.3390/atmos9020050.

Varentsov, M.I., Konstantinov, P.I., Shartova, N.V., Samsonov, T.E., Kargashin, P.E., Varentsov, A.I., Fenner, D., Meier, F., 2020a. Urban heat island of the Moscow megacity: the long-term trends and new approaches for monitoring and research based on crowdsourcing data. IOP Conf. Ser. Earth Environ. Sci. 606, 012063 https://doi.org/10.1088/1755-1315/606/1/012063.

Varentsov, M., Samsonov, T., Demuzere, M., 2020b. Impact of urban canopy parameters on a Megacity’s Modelled thermal environment. Atmosphere 11 (12), 1349. https://doi.org/10.3390/atmos11121349.

Weber, R.O., Talkner, P., 2001. Spectra and correlations of climate data from days to decades. J. Geophys. Res.-Atmos. 106 (D17), 20131–20144. https://doi.org/10.1029/2001JD000548.

Wilby, R.L., 2003. Past and projected trends in London’s urban heat island. Weather 58 (7), 251–260. https://doi.org/10.1256/wea.183.02.

Wilson, B.C., Sevick, E.M., Patterson, M.S., Chance, B., 1992. Time-dependent optical spectroscopy and imaging for biomedical applications. Proc. IEEE 80 (6), 918–930. https://doi.org/10.1109/5.149454.

Wu, J., Zha, J., Zhao, D., Yang, Q., 2018. Changes in terrestrial near-surface wind speed and their possible causes : an overview western North Pacific. Clim. Dyn. 51 (5), 2039–2078. https://doi.org/10.1007/s00382-017-3997-y.

Yang, J., Bou-Zeid, E., 2018. Should cities embrace their heat islands as shields from extreme cold? J. Appl. Meteorol. Climatol. 57 (6), 1309–1320. https://doi.org/10.1175/JAMC-D-17-0265.1.

Yang, P., Ren, G., Liu, W., 2013. Spatial and temporal characteristics of Beijing urban heat island intensity. J. Appl. Meteorol. Climatol. 52 (8), 1803–1816. https://doi.org/10.1175/JAMC-D-13-0125.1.

Yushkov, V.P., Kurbatova, M.M., Varentsov, M.I., Lezina, E.A., Kurbatov, G.A., Miller, E.A., Repina, I.A., Artamonov, A.Y., Kallistratova, M.A., 2019. Modeling an Urban Heat Island during Extreme Frost in Moscow in January 2017. Izvestiya. Atmos. Oceanic Phys. 55 (5), 389–406. https://doi.org/10.1134/S0001433819050128.